Fcc/Hcp Martensitic Transformation in the Fe-Mn System: Experimental Study and Thermodynamic Analysis of Phase Stability

S. COTES, M. SADE, and A. FERNÁNDEZ GUILLERMET

A new experimental study of A_s and M_s in the Fe-Mn system has been performed by using two complementary experimental techniques, *viz.,* dilatometry and electrical resistivity measurements, which are applied to the whole composition range where the transformation can be detected, *i.e.,* between 10 and 30 pct Mn. We used the A_s and M_s temperatures as input information in an analysis based on thermodynamic models for the Gibbs energy of the face-centered cubic (fcc) and hexagonal close-packed (hcp) phases. In these models, the magnetic contribution to Gibbs energy is accounted for, which allows us to study, by calculation, the influence of the entropy of magnetic ordering upon the relative stability of the phases. The picture of magnetic effects upon the fcc/hcp transformation that emerges from our work is as follows. At low Mn contents, the martensitic transformation temperatures are larger than the Néel temperature of the fcc phase, and both A_s and M_s decrease linearly with increasing Mn. This encourages an extrapolation to zero Mn content, and we use that to critically discuss the available information on the fcc/hcp equilibrium temperature for Fe at atmospheric pressure. At sufficiently large Mn contents, we have $M_s < T_N$, which implies that the fcc phase orders antiferromagnetically before transforming to the hcp phase. Since hcp remains paramagnetic down to lower temperatures, the ordering reaction in fcc leads to a relative stabilization of this phase, which is reflected in a drastic, nonlinear decrease of M_s.

I. INTRODUCTION

IT has long been known that a metastable hexagonal close-packed (hcp) structure, so-called ε phase, can be obtained at low temperatures by rapidly cooling the face-centered cubic (fcc)-(γ) structure alloys of the Fe-Mn system.[1–6] The transformation between γ and ε is martensitic,[4] and there is an extensive literature devoted to the ε martensite, the systematics of its occurrence, and its influence upon the properties of the material.[6–23] The interest in this system has been renewed since it was reported[25] that Fe-Mn alloys show the so-called shape-memory effect (SME), which is governed by the fcc $\leftrightarrow$ hcp martensitic transformation. A significant observation of the former studies is that the SME in this system is not strong, and it deteriorates at sufficiently large Mn content. Since this affects the possible technical applications of these alloys, there has been a considerable interest in the search for methods to improve the SME in alloys based on Fe-Mn. Much of the work reported during the last decade has been devoted to the effect of adding Si to the binary system,[26–40] but other ternary, quaternary, and quinary alloys of various compositions have been studied experimentally.[41–45] The test of specific multicomponent alloys provides useful information for the design of new materials with SME, but the search for a detailed understanding of this effect demands a more systematic approach. It seems necessary first to focus on the behavior of the Fe-Mn system, then proceed with the relevant ternary systems, and finally consider the quaternary and higher-order alloys. This methodology has proved to be very useful in the field of thermodynamic modeling of multicomponent phase diagrams,[46] and it should be interesting to explore its possibilities in treating the martensitic transformation in alloys of the type Fe-Mn-X.

A traditional start point in the theoretical analysis of the martensitic transformation is the consideration of the relative stabilities of the phases, which can be described thermodynamically in terms of Gibbs energy functions, G_m.[47] These functions are usually evaluated from thermochemical measurements on the various structures and information about the phase diagram.[47,48] However, the Fe-Mn fcc structure is not a stable phase at the temperatures where the martensitic transformation occurs, and the hcp phase is metastable at all temperatures in this system, which makes it necessary to look for additional sources of thermodynamic information. In the present work, we study the composition dependence of the phase stabilities by relying on experimental data about the temperatures for the start of the $\gamma \rightarrow \varepsilon$ (M_s) and $\varepsilon \rightarrow \gamma$ (A_s) martensitic transformations, and the concept of T_0 temperature, used earlier by Kaufman and Cohen.[47] The T_0 temperature cannot, in general, be determined directly, but it can be approximated from values for the M_s and A_s temperatures.[47,48] Our survey of the information available on the Fe-Mn system reveals, in agreement with previous reviews,[6] a large scatter in the A_s and M_s and significant discrepancies between the results of the various authors. Therefore, we have performed an experimental study of the M_s and A_s temperatures in the Fe-Mn system.

The experimental part of the present work concerns al-

S. COTES, Graduate Student, and M. SADE, Permanent Staff, are with the Centro Atómico Bariloche, Comisión Nacional de Energía Atómica, 8400 Bariloche, Argentina. A. FERNÁNDEZ GUILLERMET, Permanent Staff, is with the Consejo Nacional de Investigaciones Científicas y Técnicos (CONICET), Argentina, and the Centro Atómico Bariloche, Comisión Nacional de Energía Atómica, 8400 Bariloche, Argentina.

Manuscript submitted December 13, 1993.

loys with Mn contents between 10 and 30 wt pct, which covers the composition range where the hcp structure has previously been detected. The transformation is studied by using a combination of electrical-resistivity and dilatometric measurements. The T_0 values obtained from our measurements are used as input data in a thermodynamic analysis, which is based on mathematical models for G_m. A previous thermodynamic study by Rabinkin[49] suggested that magnetic effects, associated to the paramagnetic → antiferromagnetic transition in the fcc structure, might be responsible for the relative stabilization of the γ phase at large Mn contents. By using early descriptions of the thermodynamics of Fe,[50,51] Mn,[52] and the fcc and hcp solid-solution phases,[53] Rabinkin[49] accounted qualitatively for the trends in the T_0 values according to some authors[12,18,21] but predicted a possible fcc/hcp transformation for Mn contents larger than those reported. The present investigation of the magnetic effects upon phase stabilities relies on more recent information about the thermodynamics of Fe,[54] Mn,[55] the thermochemistry of the fcc Fe-Mn phase,[56] and an account of the magnetic contribution to G_m of the fcc and hcp phases, which is based on a model due to Inden,[57] and Hillert and Jarl.[58] In addition, we use the T_0 values for Fe-Mn alloys to gain information about the temperature for the fcc + hcp two-phase equilibrium in pure Fe at atmospheric pressure. Both modifications of Fe are metastable at ambient conditions, but the (metastable) fcc/hcp equilibrium temperature can be predicted by calculation, using a thermodynamic description of the pressure-temperature phase diagram of Fe. Such procedures has previously been applied, but the reported equilibrium temperatures[51,54] show a considerable discrepancy.[59]

II. EXPERIMENTAL TECHNIQUES

A. *Alloys, Specimens, and Heat Treatments*

The alloys used in this study were made of electrolytic iron and manganese of 99.9 pct purity. They were arc-melted under an Ar pressure of 350 mm Hg. A Cu crucible refrigerated with water was used. Mechanical pump vacuum (1.9 mm Hg) was obtained before introducing Ar up to a pressure of 160 mm Hg in the furnace chamber. This procedure was repeated at least three times before melting the alloys under the selected final Ar pressure. Once the final conditions were obtained, and in order to absorb the possible O_2 left, a piece of pure Ti was melted before the Fe-Mn alloys. Special care was taken to avoid Mn evaporation. This was achieved by adopting an arrangement of the pure metals that allowed to melt the Fe first, which then acted as a closed box for the Mn. After melting, the pressure in the chamber increased between 20 and 50 mm Hg only, which corroborated that Mn evaporation was significantly inhibited. Each alloy was melted five times to increase its homogeneity. The weight of the alloys was about 30 g, and the weight loss was 1 g in the alloy Fe-27.7 wt pct Mn (alloy number 10 in Table I) and between 0.3 and 0.6 g in the other alloys.

Each alloy was encapsulated in quartz under Ar atmosphere, kept 48 hours at 1273 K, and then quenched in water at room temperature, breaking the capsule. Air cooling was used for alloy numbers 6 and 10 in Table I. From each alloy, samples were prepared using a spark cutter. Plates of 25 × 3 × 1 mm were used for resistivity measurements, and samples with a rectangular cross section of 5 × 3 mm and 10-mm height were prepared for dilatometric measurements. Cylindrical samples of 12-mm length and 2-mm diameter were also mechanically prepared for additional dilatometric measurements. The samples were encapsulated separately in quartz under Ar pressure, heat-treated 1 hour at 1273 K, and then quenched in water, breaking the capsule. The specimens were mechanically polished using 600-grit paper and chemically polished using a 50 pct solution of HPO_3 in H_2O_2.

The analysis of chemical composition was performed for each alloy used in this work. Analysis using a wave dispersion spectrometer (WDS) was used for every alloy, and two additional methods were applied to check the first technique for alloy numbers 6 and 10 (Table I). These were neutron activation and atomic absorption for Mn content. The composition analysis was performed on small pieces obtained from the samples, which were used for resistivity measurements. For example, Figure 1 shows the way in which the samples were selected for the neutron activation analysis of alloy numbers 6 and 10. The results, which are presented in Table II, suggest that a high degree of homogeneity has been achieved in the present alloys. The WDS technique was applied with a PHILIPS* electron microprobe. Each sample to be analyzed was included with the reference pure metals in the same acrylic button, and the surface was polished up to a diamond grain of 0.25 μm. The composition of the alloys determined in this way are given in Table I.

*PHILIPS is a trademark of Philips Electronics Instrument Corp., Mahwah, NJ.

B. *Dilatometric and Electrical Resistivity Methods*

Electrical resistivity measurements were performed in a criostat that allowed a controlled temperature change between 86 and 573 K. The temperature of the sample was measured by means of a Ni-Cr vs. Ni-Al thermocouple welded on its surface. A direct current of 150 mA was used, and the potential drop was measured by means of a 148 Keithley nanovoltmeter. Heating and cooling rates of about 3 K/min were used in these measurements.

Dilatometric measurements were performed by using two different dilatometers, one with a temperature range from 103 to 623 K and a commercial dilatometer, Adamel Lhomargy. In both equipments, the specimen is connected to a linear variable differential transformer (LVDT) *via* a quartz tube. In the first one, a LVDT-type Hottinger W1E was used. The resolution of both systems is 10^{-4} mm. A thermocouple was welded on the surface of the samples. A heating rate of 3 K/min was used for all the samples measured in the first mentioned dilatometer. Samples of alloys 1 and 2 were measured with the Adamel equipment, with two different heating rates depending on the maximum desired temperature, *viz.*, a rate of 0.6 K/s was used when the maximum temperature was lower than 623 K and 1.25 K/s for higher temperatures.

To determine the martensitic transformation temperatures, the ratios $\Delta\rho/\rho_0 = [\rho(T) - \rho(T_R)]/\rho(T_R)$ and $\Delta\ell/\ell_0 = [l(T) - l(T_R)] / l(T_R)$, where T_R is room temperature, were studied as functions of T. The A_s and M_s temperatures were

Table I. Martensitic Transformation Temperatures Obtained in the Present Work (With the Mn Content of the Alloys Determined by Microprobe Measurements Using a Wave Dispersion Spectrometer (WDS))

		Electrical Resistivity				Dilatometry			
		First Cycle		Second Cycle		First Cycle		Second Cycle	
Alloy No.	Wt Pct Mn (WDS)	M_s (K)	A_s (K)	M_s (K)	A_s (K)	M_s (K)	A_s (K)	M_s (K)	A_s (K)
1	10.2 ± 0.2	—	—	—	—	—	—	—	—
2	13.7 ± 0.6	—	—	—	—	421.7	496	416.2	489.2
3	15.9 ± 1.0	432	480.8	426	488.6	444	482.4	439.7	485.5
4	19.3 ± 0.4	401.2	470.3	394.7	476	417.5	471	X	X
5	21.9 ± 0.4	395.7	439	404.2	445.3	375.9	449.7	X	X
6*	24.7 ± 0.8	380	438	375.7	443.7	371.6	446	365.4	448.5
7	25.1 ± 0.6	329.4**	435	302	439	333.7	425.2	316.2	421.5
8	26.5 ± 0.1	—	423	—	—	292.4	424	269.7	424
9	27.3 ± 0.3	303**	416	X	X	268.5	422.8	259	417.8
10	27.7 ± 0.7	307**	416	—	420.5	—	414	—	—
11	29.3 ± 1.3	253**	417	—	419	280.5	411.7	—	409.2
12	30.6 ± 0.5	—	—	—	—	—	—	—	—

Notes: X, not measured; —, not observed in the experiment.
*Additional cycles in electrical resistivity measurements gave the following values:

Cycle	M_s (K)	A_s (K)
3rd	377	444
4th	374	445
26th	373	458

**See Section III–A–3.

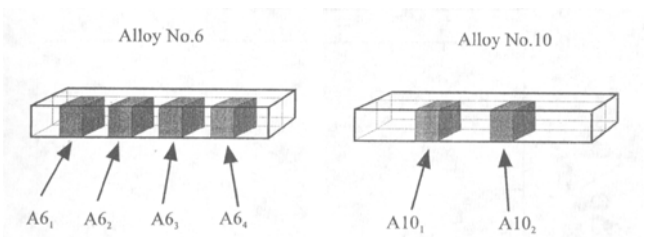

Fig. 1—Diagram showing how the alloy pieces needed for the neutron activation determination of the chemical composition were cut from the samples used for electrical resistivity measurements. The results of the analysis are given in Table II.

Table II. The Mn Content of Various Samples Taken from Alloys 6 and 10 (Figure 1), as Determined by Neutron Activation Analysis

Alloy No.	Sample	Weight (mg)	Wt Pct Mn
6	$A6_1$	3.011 ± 0.01	23.5 ± 0.3
	$A6_2$	2.788 ± 0.01	23.5 ± 0.3
	$A6_3$	3.081 ± 0.01	23.1 ± 0.6
	$A6_4$	0.320 ± 0.01	23.9 ± 0.8
10	$A10_1$	2.711 ± 0.01	27.7 ± 0.3
	$A10_2$	2.523 ± 0.01	27.6 ± 0.3

obtained by analyzing the variations in the slope in $\Delta\rho/\rho_0$ *vs* T and $\Delta\ell/\ell_0$ *vs* T plots. This was, in general, performed by visual examination, but in certain cases, the derivatives of the $\Delta\rho/\rho_0$ *vs* T and $\Delta\ell/\ell_0$ *vs* T functions were considered as well.

C. *Optical Microscopy and Neutron Diffraction Experiments*

Metallographic observations were performed on several samples. Those were mechanically and chemically polished using a 5 pct solution of nitric acid in etilic alcohol. The usual morphologies[60] of the (γ) and (ε) phases were observed. The melting procedure of the present alloys led, in general, to γ-phase grains of a columnar type. Estimates of the average grain size were obtained by line analysis on an optical microscope. Examination of alloys 3, 4, 7, 9 and 12 indicated that the smallest grain diameter was comprised between 94 and 132 μm. In addition, neutron diffraction experiments were carried out to accurately establish the constitution of the experimental alloys as well as to determine the lattice parameters of the various phases as a function of the Mn content.[61]

III. MARTENSITIC AND MAGNETIC TRANSFORMATION TEMPERATURES

A. *Analysis of Electrical Resistivity Data*

The results (Table I) will be discussed by grouping the alloys according to their behavior. In the rest of this work, the composition of the alloys is given in weight percent. In each case, the heating of the sample was performed first, and the sample was cooled afterward to the lowest desired temperature.

1. *Alloys 3 (15.9 pct Mn), 4 (19.3 pct Mn), and 5 (21.9 pct Mn)*

Figure 2 shows the $\Delta\rho/\rho_0$ *vs* T curves for alloy 4 (19.3 pct Mn), corresponding to the first and second cycles. At low temperatures, a mixture of γ and ε is expected.[22] The abrupt change in slope observed at T = 470.3 K corresponds to the start of the $\varepsilon \rightarrow \gamma$ transformation. For temperatures lower than M_f, no structural changes are determined through resistivity measurements, but the material is only partially transformed.[62] A small difference between the values obtained before and after heating (points a and c in Figure 2(a)) was obtained in the first cycle, indicative

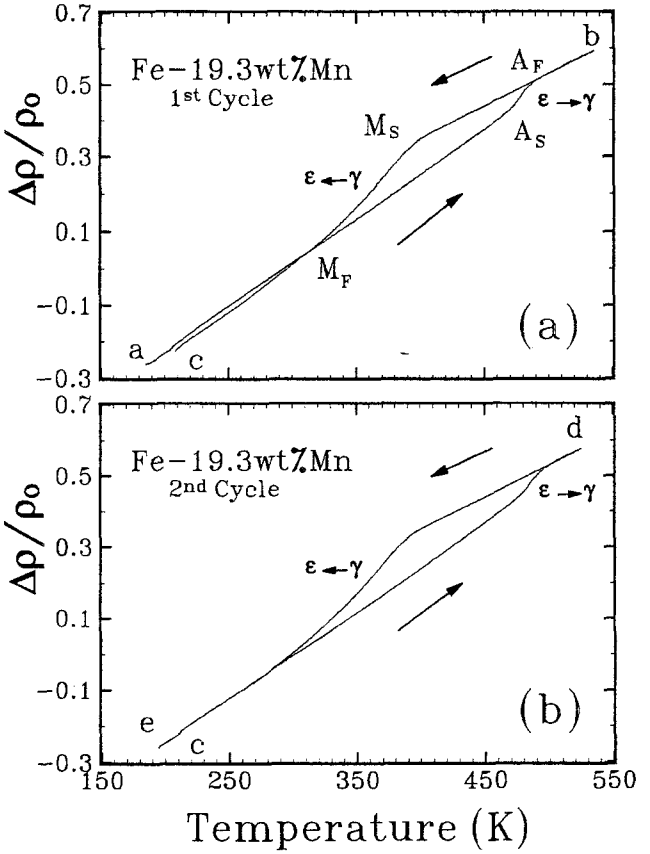

Fig. 2—Electrical resistivity *vs* temperature data for the Fe-19.3 pct Mn alloy, obtained on heating and cooling during (a) the first thermal cycle and (b) the second cycle.

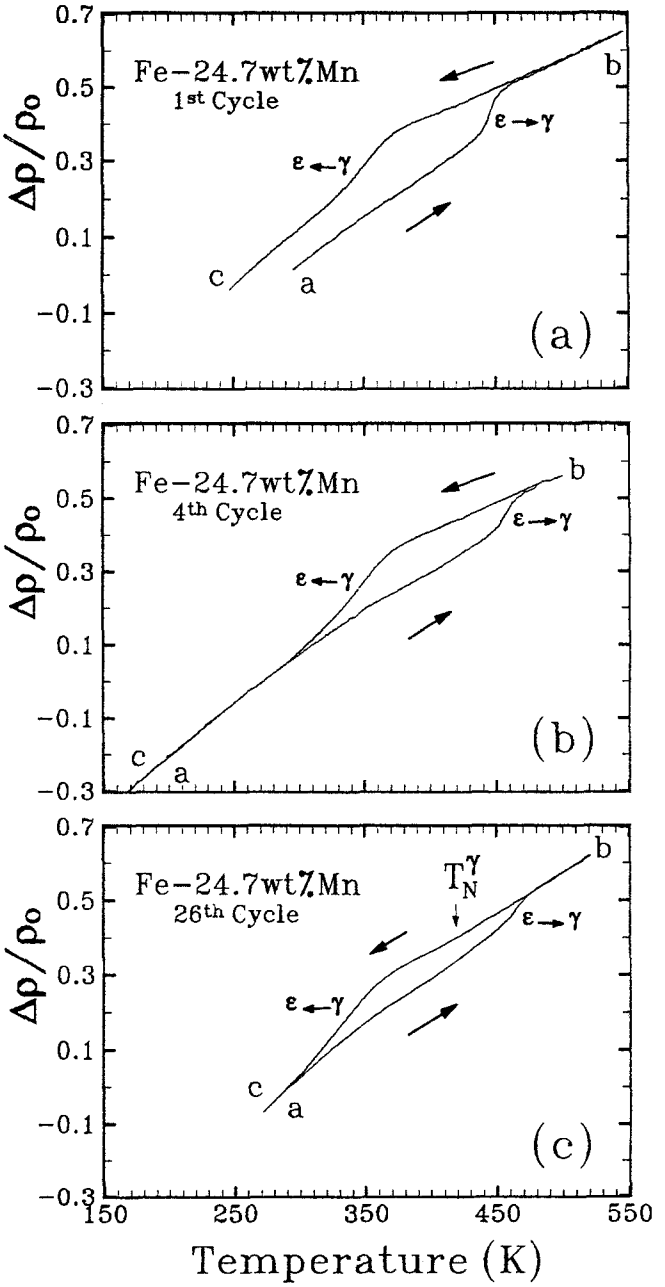

Fig. 3—Electrical resistivity *vs* temperature data for the Fe-24.7 pct Mn alloy, obtained on heating and cooling during (a) the first, (b) the fourth, and (c) the 26th thermal cycle.

of some hysteresis for temperatures lower than M_f. This shows that the amount of martensite present in the sample at the states represented by points "a" and "c" was different. The effect was not observed in the second cycle (Figure 2(b)).

2. *Alloys 6 (24.7 pct Mn) and 7 (25.1 pct Mn)*

The $\Delta\rho/\rho_0$ *vs* T curves for the 1st, 4th, and 26th cycle for alloy 6 are shown in Figure 3. Figure 3(a) shows that the variation in resistivity due to the $\gamma \rightarrow \varepsilon$ transformation is smaller than the corresponding to the retransformation and that hysteresis is observed for temperatures lower than M_f. Closed loops were obtained in the following cycles, but the transformation temperatures did not remain constant (see the numerical values at the bottom of Table I). After the fourth cycle, additional thermal cycling was performed between liquid nitrogen temperature and 573 K. In particular, the $\Delta\rho/\rho_0$ *vs* T curve for the 26th cycle was determined (Figure 3(c)). A small decrease in M_s and an increase in A_s was then observed (see values in Table I), and it was found that the magnitude of the resistivity change due to the $\gamma \rightarrow \varepsilon$ transformation decreases with cycling; *i.e.,* the amount of martensite formed on cooling decreases with increasing number of cycles. The change in slope detected at a temperature higher than M_s corresponds to the paramagnetic to antiferromagnetic transformation in the γ phase,[63] which is indicated as T_N^{γ} in Figure 3(c).

Alloy 7 (Fe-25.1 pct Mn) presented an analogous behavior, but the M_s value from electrical resistivity that is given for this alloy in Table I was determined by another method, which is described in detail in the next subsection.

3. *Alloys 8 (26.5 pct Mn), 9 (27.3 pct Mn), 10 (27.7 pct Mn), and 11 (29.3 pct Mn)*

Figure 4 shows the $\Delta\rho/\rho_0$ *vs* T curves obtained in the first and second cycles of alloy 11 (29.3 pct Mn). From the first heating curve (line ab in Figure 4(a)) the A_s temperature can be easily determined. On cooling from the γ state (point b, Figure 4(a)) a change in slope of the type expected for the magnetic transformation in γ is observed, which is denoted as T_N^{γ}. However, the superposition of the $\varepsilon \rightarrow \gamma$ and the magnetic transformation hinders an accurate determination of T_N^{γ} from the heating curve obtained in the first cycle.

The existence of hysteresis in Figure 4 and in similar

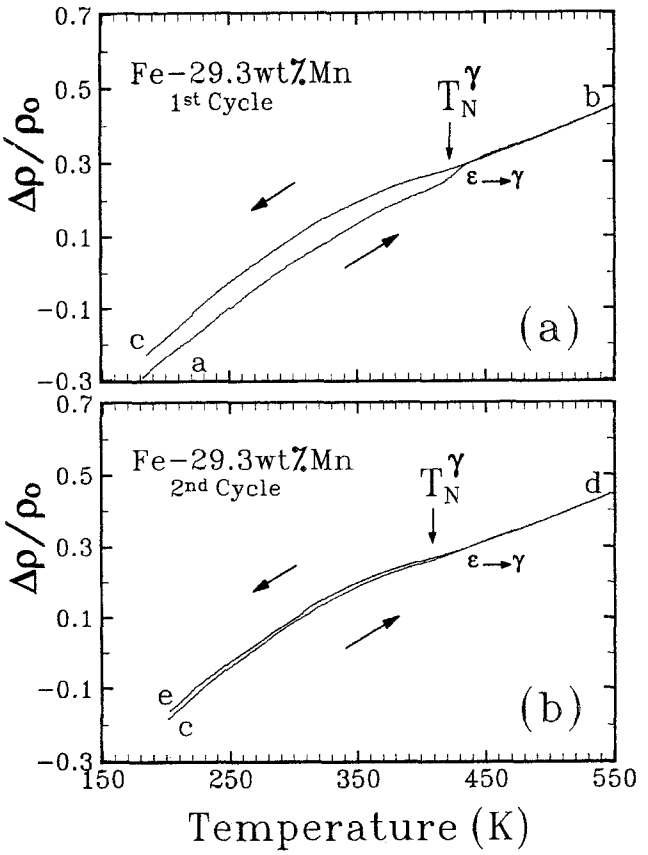

Fig. 4—Electrical resistivity *vs* temperature data for the Fe-29.3 pct Mn alloy, obtained on heating and cooling during (a) the first and (b) the second thermal cycle.

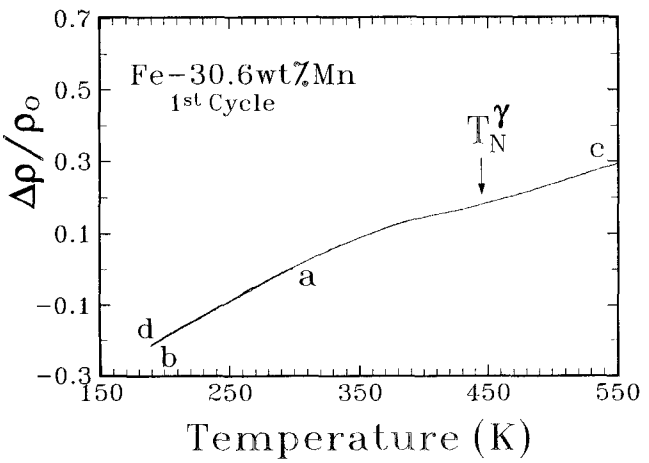

Fig. 5—Electrical resistivity *vs* temperature data for the Fe-30.6 pct Mn alloy, obtained on heating and cooling during the first thermal cycle.

results for the Fe-26.5 pct Mn, Fe-27.3 pct Mn, and Fe-27.7 pct Mn alloys demonstrates that a structural transformation took place on cooling. However, the M_s temperatures could not be determined from cooling curves of the type shown in Figure 4. The following procedure was adopted. The samples were subjected to thermal cycling in the temperature range $[T, A_f]$, where T for cycle $N + 1$ was lower than T for cycle N. In this way, no hysteresis was present during the cycles for which $T > M_s$ and appeared once $T < M_s$. This method allowed us to bracket the start of the $\gamma \rightarrow \varepsilon$ transformation and to obtain a reasonably

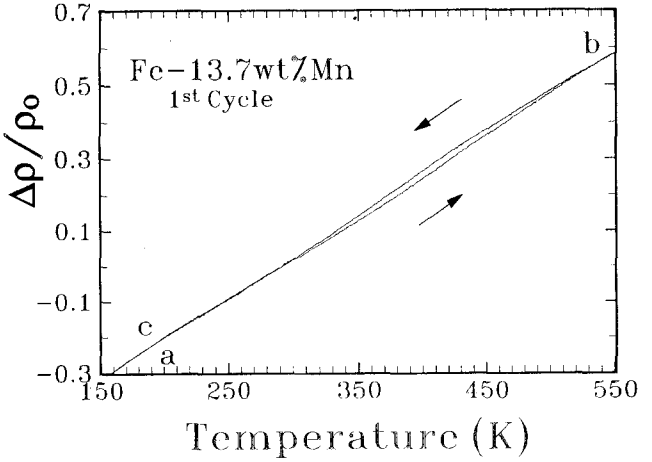

Fig. 6—Electrical resistivity *vs* temperature data for the Fe-13.7 pct Mn alloy, obtained on heating and cooling during the first thermal cycle.

accurate estimate of M_s for the Fe-25.1 pct Mn, Fe-27.3 pct Mn, Fe-27.7 pct Mn and Fe-29.3 pct Mn alloys. No M_s was detected in this way for the Fe-26.5 pct Mn alloy when $T > 300$ K. Additional information was obtained from dilatometric measurements, which are reported in Section B.

Finally, we should comment on the appreciable $\varepsilon \rightarrow \gamma$ transformation observed in Figure 4(a). Since the results of the second cycle (Figure 4(b)) and the following cycles demonstrate that thermally induced martensite is not easily formed in alloys of this composition, we suggest that the ε-martensite responsible for the effect in Figure 4(a) has another origin. In particular, the handling of the sample before the first cycle might have introduced stress-induced martensite, which is known to occur in Fe-Mn alloys.[16] This explanation is consistent with our other experimental results.[64]

4. *Alloy 12 (30.6 pct Mn)*

The $\Delta\rho/\rho_0$ *vs* T curves corresponding to alloy 12 (30.6 pct Mn) (Figure 5) show that no hysteresis is observed with an uncertainty in the resistivity values corresponding to the thickness of the line, but the magnetic order-disorder transition is well detected. Previous studies of the martensitic transformation in the Fe-Mn system show that the amount of ε phase formed on cooling decreases with increasing Mn content.[9] The decrease in the width of the hysteresis loop observed when going from the alloy with 19.3 pct Mn (Figure 2) to 24.7 pct Mn (Figure 3) and to 29.3 pct Mn (Figure 4) also led us to expect an even narrower hysteresis loop for the alloy with 30.6 pct Mn, which is observed. In addition, the lack of detectable hysteresis for the Fe-30.6 pct Mn alloy adds to the significance of the small hysteresis observed in alloys with lower Mn contents, *e.g.,* in Figure 4.

5. *Alloys 1 (10.2 pct Mn) and 2 (13.7 pct Mn)*

The $\Delta\rho/\rho_0$ *vs* T curve for alloy 2 (13.7 pct Mn) is shown in Figure 6. In Fe-Mn alloys with Mn content lower than 18 pct, a body-centered cubic (bcc) phase has been reported, often called the α phase, which forms martensitically on cooling,[12] and hinders the formation of ε. However, the existence of a closed loop at temperatures lower than the known $A_s^{\alpha\rightarrow\gamma}$ [6] of this alloy indicates that ε martensite is indeed formed. Its transformation temperatures were measured using dilatometric techniques, as explained in the next subsection.

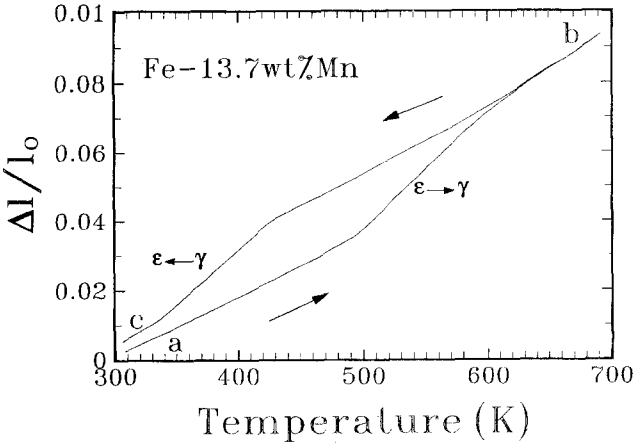

Fig. 7—Thermal expansion *vs* temperature data for the Fe-13.7 pct Mn alloy, obtained on heating and cooling during the first thermal cycle, in the temperature range of the $\gamma \leftrightarrow \varepsilon$ martensitic transformation.

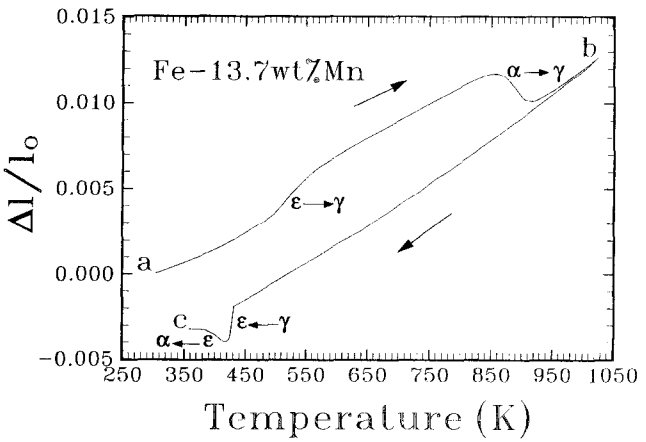

Fig. 8—Thermal expansion *vs* temperature data for the Fe-13.7 pct Mn alloy, obtained on heating and cooling in a temperature range that involves both the $\gamma \leftrightarrow \varepsilon$ and the $\alpha \rightarrow \gamma$ martensitic transformations.

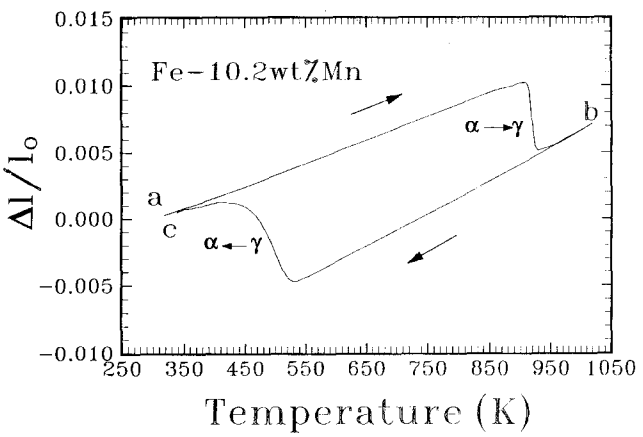

Fig. 9—Thermal expansion *vs* temperature data for the Fe-10.2 pct Mn alloy, obtained on heating and cooling during the first thermal cycle.

No hysteresis was found for alloy 1 (10.2 pct Mn) in the temperature range from 123 to 573 K.

B. *Analysis of Dilatometric Measurements*

Figure 7 shows the dilatometric curve for alloy 2 (13.7 pct Mn) corresponding to a thermal cycle between room temperature and 693 K. The A_s and M_s temperatures are now better defined than in the resistivity measurements in Figure 6. To determine if at room temperature α martensite is present together with the ε phase, an additional heating to 1043 K was performed , and the corresponding $\Delta\ell/\ell_0$ *vs* T curve is shown in Figure 8. On heating from room temperature (point a in the figure), an expansion takes place, which accounts for the $\varepsilon \rightarrow \gamma$ transformation. On further heating, a contraction is observed, which can be related to the $\alpha \rightarrow \gamma$ transformation. This implies that $A_s^{\alpha \rightarrow \gamma} = 859$ K, which is in agreement with previously reported[6] values. The first abrupt change in slope observed on cooling is a contraction, indicating the $M_s^{\gamma \rightarrow \varepsilon}$ temperature. The expansion of the sample, at about 420 K, is explained by the formation of α phase. Both martensitic structures ε and α coexist at room temperature in this alloy.

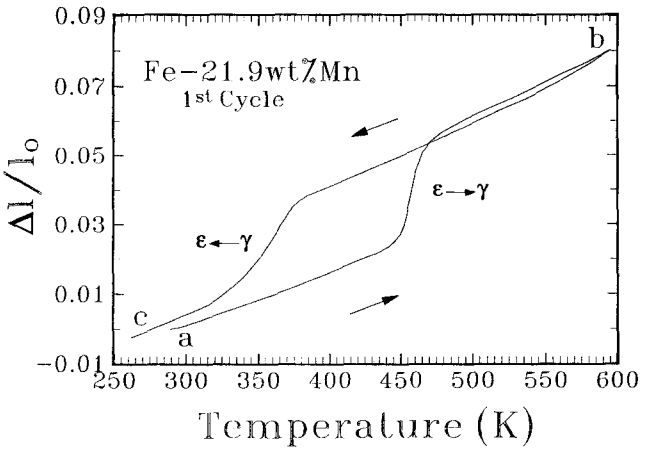

Fig. 10—Thermal expansion *vs* temperature data for the Fe-21.9 pct Mn alloy, obtained on heating and cooling during the first thermal cycle.

Dilatometric measurements performed on the Fe-10.2 pct Mn alloy between room temperature and 693 K showed no hysteresis, but a thermal cycle between room temperature and 1043 K (Figure 9) showed a closed loop, with an expansion on heating starting at $T = 911$ K and a contraction on cooling starting at $T = 524$ K. These temperatures were taken as the $A_s^{\alpha \rightarrow \gamma}$ and $M_s^{\gamma \rightarrow \alpha}$ values, respectively.

Complementary dilatometric measurements were also performed on the other alloys of Table I. Figure 10 shows the first cycle of alloy 5 (Fe-21.9 pct Mn). No information from the magnetic ordering of the γ phase is obtained from this curve because of the overlap of the $\gamma \rightarrow \varepsilon$ transformation temperature with T_N^{γ}. The first two thermal cycles of alloy 6 (Fe-24.7 pct Mn) are shown in Figure 11. A decrease in M_s was observed (Table I).

The dilatometric curves corresponding to alloys 7 (Fe-25.1 pct Mn), 8 (Fe-26.5 pct Mn), 9 (Fe-27.3 pct Mn), 10 (Fe-27.7 pct Mn), and 11 (Fe-29.3 pct Mn) show that (a) the direct $\gamma \rightarrow \varepsilon$ transformation becomes more difficult to detect after the first few cycles, while the retransformation is clearly observed during several thermal cycles; (b) a higher amount of martensite is present after quenching than after the first cooling of the alloy; and (c) the magnetic transition in γ is detected. For example, dilatometric results for alloy 8 (Fe-26.5 pct Mn) are shown in Figure 12. Furthermore, Figure 13 shows the first two thermal cycles of alloy 10 (Fe-27.7 pct Mn) for temperatures higher than room temperature.

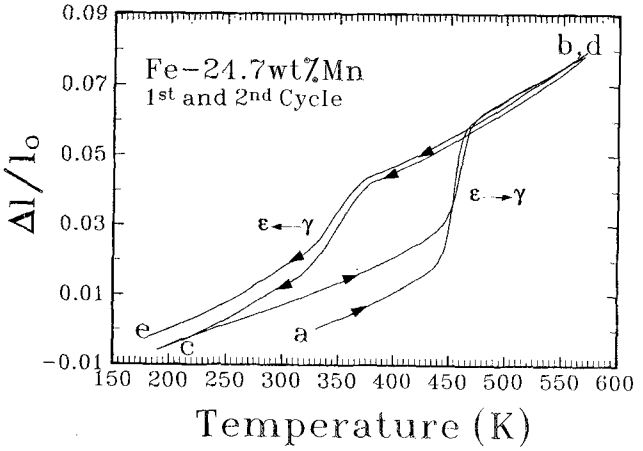

Fig. 11—Thermal expansion *vs* temperature data for the Fe-24.7 pct Mn alloy, obtained on heating and cooling during the first and second thermal cycle.

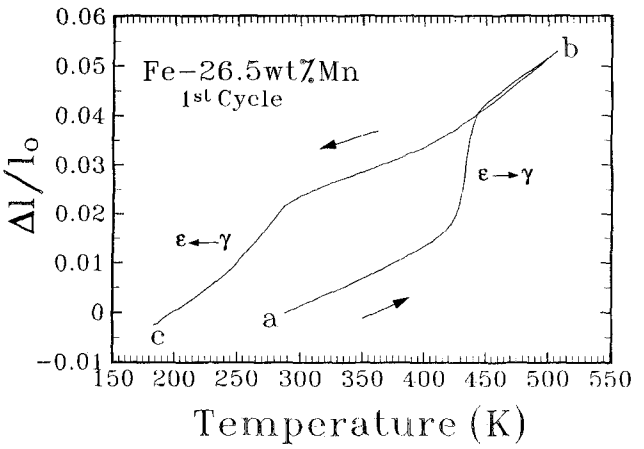

Fig. 12—Thermal expansion *vs* temperature data for the Fe-26.5 pct alloy, obtained on heating and cooling during the first thermal cycle.

IV. DISCUSSION OF THE EXPERIMENTAL RESULTS

A. *General Considerations*

A_s and M_s temperatures arrived at in this work are given in Table I and compared in Figures 14 and 15, respectively, with the results according to various authors.[4,12,17,18,22,25,62,65–74] The experimental data in these graphs scatter considerably, which further testifies to the difficulties in determining experimentally the start of the $\gamma \rightarrow \varepsilon$ and $\varepsilon \rightarrow \gamma$ martensitic transformations in this system. A documented reason for the discrepancy among the authors is the presence of impurities. There are indications[17,22] that the increase in the carbon content of the material depresses the M_s temperature of Fe-Mn alloys. Gulyaev *et al.*[22] performed dilatometric measurements in alloys with two different degrees of purity, obtained by vacuum melting and open melting, respectively, and found an effect on M_s of about 35 K. Figures 14 and 15 also illustrate the magnitude of the experimental scatter in a series of measurements based on the same technique, on alloys with comparable impurity contents. For instance, the composition dependence of the A_s values obtained by Umebayashi and Ishikawa[67] for an alloy with 21.4 pct Mn from magnetic susceptibility measurements (Figure 14) deviates negatively

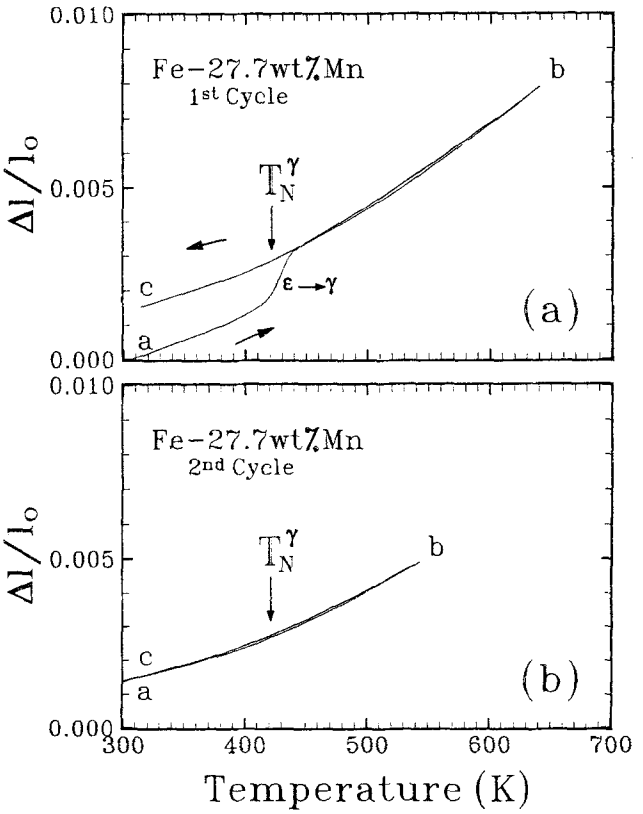

Fig. 13—Thermal expansion *vs* temperature data for the Fe-27.7 pct Mn alloy, obtained on heating and cooling during (a) the first and (b) the second thermal cycle.

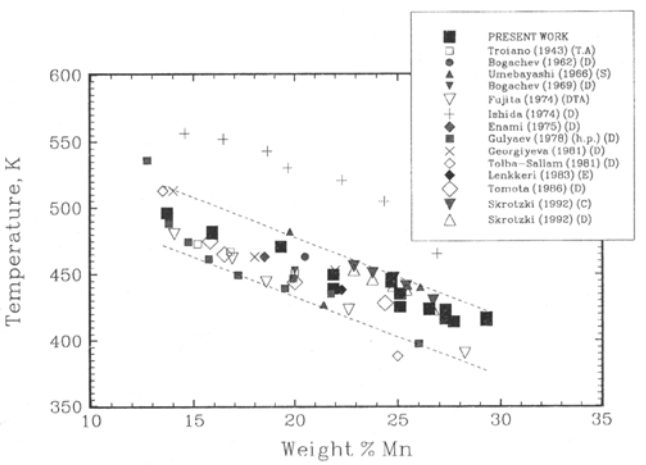

Fig. 14—The temperature A_s for the start of the $\varepsilon \rightarrow \gamma$ martensitic transformation in Fe-Mn alloys of various Mn contents, according to the present work and previous studies. The various experimental techniques used in previous work are indicated, *viz.*, calorimetry (C), dilatometry (D), differential thermal analysis (DTA), measurement of the elastic constants (E) and of the magnetic susceptibility (S), and thermal analysis (TA). The letters h.p. refer to the results obtained by Gulyaev *et al.*[22] on Fe-Mn alloys of high purity. The dashed lines determine the limits of what we have considered as the probable range of A_s values for Fe-Mn alloys.

more than 40 K from what one expects from the trend of their remaining results. Another factor that is expected to affect the experimentally determined transformation temperatures is the grain size (GS). In a recent work, Takaki *et al.*[75] showed that M_s for an Fe-15 pct Mn alloy decreases rapidly with the GS if the size of the austenite grain is

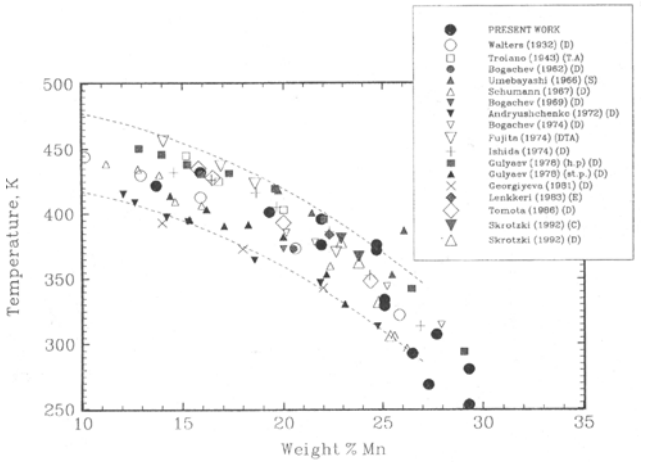

Fig. 15—The temperature M_s for the start of the $\gamma \rightarrow \varepsilon$ martensitic transformation in Fe-Mn alloys of various Mn contents, according to the present work and previous studies. The various experimental techniques used in previous work are indicated, *viz.*, calorimetry (C), dilatometry (D), differential thermal analysis (DTA), measurements of the elastic constants (E) and of the magnetic susceptibility (S), and thermal analysis (TA). The letters h.p. and st.p. refer to the results obtained by Gulyaev *et al.* [22] on Fe-Mn alloys of high purity and standard purity, respectively. The dashed lines determine the limits of what we have considered as the probable range of M_s values for Fe-Mn alloys.

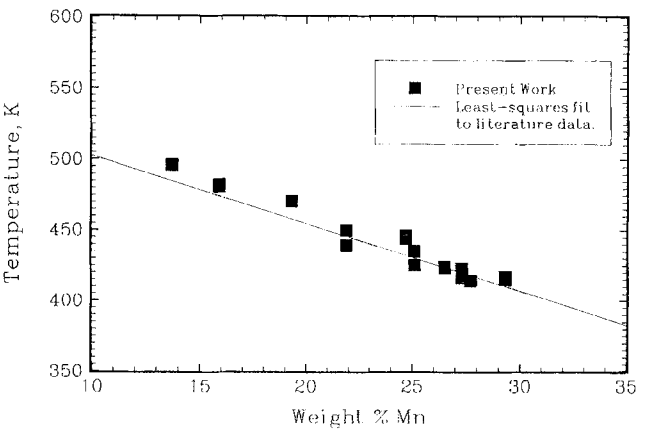

Fig. 16—The results of a least-squares fit to those A_s *vs* pct Mn values from the literature that fall in the scatter band of Fig. 14 (solid line) compared with the A_s values determined in the present work (symbols).

smaller than about 30 μm but is weakly dependent upon GS when the size of the austenite grain is larger. The GS of the alloys studied in the present work (Section II–C) falls in the latter range, and thus the present M_s transformation temperatures should be taken as essentially insensitive to small variations in GS. Finally, the martensitic transformation temperatures are also expected to depend upon the density of the crystal defects introduced during the preparation of the samples or the thermal cycling. A systematic study of this effect is in progress.[64] In summary, there is not enough information to accurately discuss the discrepancies in the data from the literature, but it is evident that the majority of the reported A_s and M_s fall in scatter bands corresponding to a maximum uncertainty of 45 K in A_s and 60 K in M_s. These bands, which are indicated by using dashed lines in Figures 14 and 15, are proposed here as a natural way to describe the range of probable transformation temperatures. Following this criterion, the A_s data presented by Ishida and Nishizawa[70] will be considered as too high.

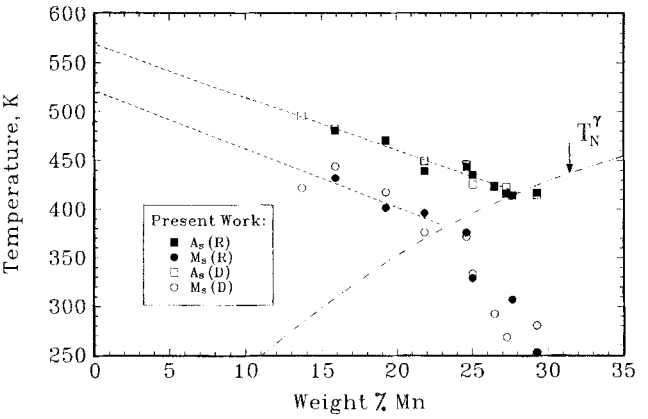

Fig. 17—The composition dependence of the A_s and M_s temperatures determined in the present work (symbols) by using dilatometric (D) and electrical resistivity measurements (R). The dashed-dotted line labeled T_N^γ gives the composition dependence of the Néel temperature of the fcc phase according to the phenomenological representation reported by Huang.[56] The two dashed straight lines refer to the results of a least-squares treatment of the A_s *vs* pct Mn data (*i.e.*, Eq. [1]) and M_s *vs* pct Mn data (*i.e.*, Eq. [3]), corresponding to compositions where $A_s > T_N^\gamma$ and $M_s > T_N^\gamma$.

B. *Composition Dependence of* A_s *and* M_s

Figures 14 and 15 demonstrate that the present experimental values fall in the scatter bands of the data from the literature. In particular, a least-squares treatment of our A_s values gives

$$A_s\,(\mathrm{K}) = (569 \pm 7) - (5.4 \pm 0.3)W_{\mathrm{Mn}} \qquad [1]$$

where W_{Mn} is weight percent Mn. This will be compared with the result of an analogous treatment of the remaining data included in the band in Figure 14, *viz.*,

$$A_s\,(\mathrm{K}) = (550 \pm 11) - (4.8 \pm 0.5)W_{\mathrm{Mn}} \qquad [2]$$

Figure 16 demonstrates that the A_s values predicted by Eq.[2] (solid line) agree very well with the present measurements (symbols), which adds to the credibility of the retransformation temperatures determined in our work.

The present M_s temperatures also fall in the scatter band of the previously published data and decrease with increasing Mn content but indicate a more complex composition dependence than that shown by A_s. We find that M_s decreases almost linearly with increasing Mn content up to about 23 pct Mn but deviates rapidly from the linear behavior between 23 and about 30 pct Mn. To gain insight into the reasons for the different behavior of A_s and M_s, we plot in Figure 17 the transformation temperatures determined in this work (symbols) and the Néel temperature of the fcc phase, T_N^γ, which we represent by using the T_N^γ *vs* weight percent Mn function proposed by Huang,[56] (Section C). In addition, we plot in Figure 17 the A_s values predicted by Eq. [1] and the M_s according to a similar least-squares treatment of the results for alloys with up to 21.9 pct Mn, which gives

$$M_s\,(\mathrm{K}) = (522 \pm 35) - (6.0 \pm 2)W_{\mathrm{Mn}} \qquad [3]$$

Figure 17 demonstrates that there is very good agreement

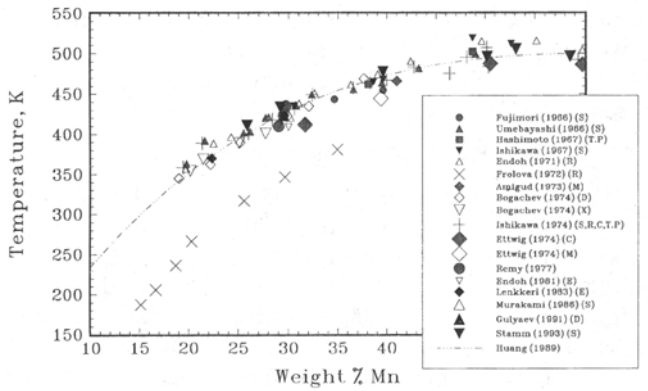

Fig. 18—The composition dependence of T_N^{γ} for the fcc phase in the Fe-Mn system according to experimental data from various authors (symbols) and the phenomenological representation reported by Huang[56] (dashed-dotted line). The various experimental techniques used in those works are indicated, *viz.*, calorimetry (C), dilatometry (D), measurements of the elastic constants (E), Mössbauer spectroscopy (M), electrical resistivity (R), magnetic susceptibility (S), thermoelectric power (T.P.), and X-ray diffraction determination of the lattice parameters (X).

between the transformation temperatures determined by the two experimental techniques used by us. From the values in Table I, we evaluate an average difference between resistivity and dilatometry of (5 ± 4) K in A_s, and (15 ± 8) K in M_s. Besides, this graphic suggests that there is a relation between the composition dependence of the transformation temperatures and the magnetic state of the fcc phase. The alloys that transform martensitically from or to the paramagnetic fcc phase show A_s and M_s temperatures that vary almost linearly with the Mn content. Alloys that transform martensitically from a magnetically ordered fcc phase show M_s temperatures that deviate rapidly from the linear behavior. Indeed, there are in Figure 17 two A_s values that fall below the Néel temperature line, but they are too close to T_N^{γ}, and no conclusion can be drawn about the magnetic effect upon the A_s *vs* percent Mn function. The rapid decrease in M_s shown by the data in Figure 17 and the fact that no ε martensite was detected in the alloy with 30.6 pct Mn (Section III) are indicative of a rapid stabilization of the fcc phase relative to hcp, and in Section V, we shall search for the origin of this effect in the thermodynamics of these phases.

C. *Composition Dependence of* T_N^{γ}

The present treatment of magnetic effects upon phase stabilities will rely on the knowledge of the Néel temperature of the fcc and hcp structures. The properties of hcp are poorly known, and in Section V–B, we explain how this phase was treated by us. In contrast with this, the Néel temperature of the fcc phase has been determined by several authors[30,39,67,73,76–87] (Figure 18). In addition, we plot in Figure 18 the T_N^{γ} *vs* composition function obtained by Huang[56] by fitting a third-degree polynomial to the data from references 67 and 77 through 79. The present dilatometric and resistivity measurements gave information about the limits of the temperature range within which the transformation took place, which were always in line with the data in Figure 18 but only for the alloys with 29.3 pct Mn and 30.6 pct Mn we obtained accurate T_N^{γ} values. Therefore, we shall base our thermodynamic treatment upon the mathematical description of T_N^{γ} due to Huang.[56]

In closing this subsection, we shall return to Figure 14. This graphic shows an experimental dilatometric data point corresponding to 25 pct Mn, due to Tolba-Sallam *et al.*,[72] which falls outside of the band of the A_s data. When heating this alloy, they observed an expansion between 388 and 433 K and interpreted these temperatures as the beginning and the end of the $\varepsilon \rightarrow \gamma$, transformation, respectively. However, we note that their lowest temperature, 388 K, is close to the Néel temperature of the alloy according to the expression by Huang,[56] *viz.*, 395 K. Besides, the highest temperature determined by Tolba-Sallam *et al.*, 433 K, compares very well with the A_s values determined in the present work for the alloy with 24.7 pct Mn, *viz.*, 438 and 446 K (Table I). Finally, the A_s value predicted by Eq. [1], 432.8 K, is also in excellent agreement with their result.

V. THERMODYNAMIC ANALYSIS

A. *Definition and Estimation of the* T_0 *Temperature*

The thermodynamic analysis of martensitic transformation temperatures at a given pressure is usually performed by invoking the concept of T_0 temperature.[47,48] Applied to the present transformation between fcc and hcp, the T_0 temperature of an alloy with a Mn content described by the atomic fraction x_{Mn} is defined by the following equation:

$$G_m^{(fcc)}(T_0, x_{Mn}) = G_m^{(hcp)}(T_0, x_{Mn}) \qquad [4]$$

where G_m is the integral Gibbs energy per mol of atoms. It is known[47] that T_0 can be estimated from experimental values of the A_s and M_s temperatures, and a frequently applied approximation[47,48] makes T_0 equal to the average of these transformation temperatures, *viz.*,

$$T_0 = \frac{A_s + M_s}{2} \qquad [5]$$

Equation [5] has often been applied to nonthermoelastic martensitic transformations, whereas for the thermoelastic case, *e.g.*, in Cu-based alloys,[88,89] T_0 has been estimated $(M_s + A_f)/2$ or $(M_f + A_s)/2$. Since the $\gamma \rightarrow \varepsilon$ martensitic transformation in Fe-Mn-X is generally[40] considered as nonthermoelastic, the simplest choice given by Eq. [5] was adopted in the present study. Then we used Eqs. [4] and [5] together with our measurements of M_s and A_s to gain thermodynamic information on the hcp phase, which is metastable in the Fe-Mn system. This method has successfully been applied to the Fe-Co[90] and Co-Ni[91] systems.

B. *Thermodynamic Modeling of Gibbs Energy*

The Gibbs energy per mole of atoms of the fcc or hcp phase was described by resolving it into a magnetic ΔG_m^{mg} and a nonmagnetic contribution, according to the following expression:

$$G_m^{\phi} = x_{Fe}\,{}^0G_{Fe}^{\phi} + x_{Mn}\,{}^0G_{Mn}^{\phi} + RT(x_{Fe} \ln x_{Fe} + x_{Mn} \ln x_{Mn}) + {}^EG_m^{\phi} + \Delta G_m^{mg,\phi} \qquad [6]$$

where x_i (i = Fe, Mn) is the atomic fraction of the element i; R is the universal gas constant; ${}^0G_i^{\phi}$ is the molar Gibbs energy of the element i, with the structure of the phase ϕ

($\phi = \gamma, \varepsilon$) in a nonmagnetic state; and ${}^{E}G_m^{\phi}$ is the excess Gibbs energy. The ${}^{0}G_i$ quantities were referred to the enthalpy of a special standard state recommended by the Scientific Group Thermodata Europe (SGTE) organization,[92] which is defined as the stable state at 298.15 K and 0.1 MPa. All necessary information about ${}^{0}G_i$ was taken from assessments of the thermodynamic properties of Fe[54] and Mn.[55,56] The magnetic contribution to G_m was described by using Hillert and Jarl's[58] modification of the model proposed by Inden,[57] which gives

$$\Delta G_m^{mg,\phi} = \mathrm{R}\ T \ln(\beta^{\phi} + 1) f^{\phi}(\tau^{\phi}) \qquad [7]$$

where β^{ϕ} is a composition-dependent parameter that is related to the total magnetic entropy, *i.e.,* the quantity $\Delta S_m^{mg,\phi}\ (\infty) - \Delta S_m^{mg,\phi}\ (0)$, as follows:

$$\Delta S_m^{mg,\phi}(\infty) - \Delta S_m^{mg,\phi}(0) = \mathrm{R} \ln(\beta^{\phi} + 1) \qquad [8]$$

The variable τ^{ϕ} is defined as T/T_c^{ϕ}, where T_c^{ϕ} is the critical temperature for magnetic ordering of the structure ϕ, *i.e.,* the Néel temperature of fcc and hcp, as a function of composition, and f^{ϕ} represents the polynomial of Hillert and Jarl.[54,55]

The variation of T_N^{γ} with Mn content was described using the expression reported by Huang.[56] According to Ohno and Mekata,[93] T_N^{ε} does not change with composition for $0.178 < x_{\mathrm{Mn}} < 0.286$. Lacking additional information, we assumed that T_N^{ε} remains constant in the whole range of interest in this work, *viz.,* $T_N^{\varepsilon} = 230$ K.[93] Following previous work,[90,91] we described the composition dependence of β^{γ} by adopting the following phenomenological expression:

$$\beta^{\gamma} = x_{\mathrm{Fe}}\, {}^{0}\beta_{\mathrm{Fe}}^{\gamma} + x_{\mathrm{Mn}}\, {}^{0}\beta_{\mathrm{Mn}}^{\gamma} - (1/3) x_{\mathrm{Fe}} x_{\mathrm{Mn}}\, \beta_{\mathrm{Fe,Mn}}^{\gamma} \qquad [9]$$

where the quantities ${}^{0}\beta_{\mathrm{Fe}}^{\gamma}$ and ${}^{0}\beta_{\mathrm{Mn}}^{\gamma}$, which refer to fcc Fe and fcc Mn, were taken from References 54 and 55, respectively. The quantity $\beta_{\mathrm{Fe,\,Mn}}^{\gamma}$ describes the deviations of the β value from the linear interpolation between the ${}^{0}\beta$ for the pure elements. This quantity is discussed in detail in Section V.D. Since a β *vs* x_{Mn} function for the hcp phase has not yet been determined experimentally, we used the composition-independent value $\beta^{\varepsilon} = 0.25$, which was estimated by adopting the Weiss and Tauer[94,95] approximation $\beta^{\varepsilon} = n_B^{\varepsilon}$ and the experimental[93] magnetic moment n_B^{ε}. This will not affect the conclusions of our study, because the present calculations concern only temperatures higher than the Néel temperature of the ε phase.

The excess Gibbs energy term ${}^{E}G_m^{\phi}$ in Eq. [6] was treated by adopting the subregular approximation of the Redlich–Kister[96] power series, *viz.,*

$${}^{E}G_m^{\phi} = x_{\mathrm{Fe}} x_{\mathrm{Mn}} [{}^{0}L^{\phi} + {}^{1}L^{\phi}(x_{\mathrm{Fe}} - x_{\mathrm{Mn}})] \qquad [10]$$

The interaction parameters ${}^{0}L^{\gamma}$ and ${}^{1}L^{\gamma}$ have been studied by Huang[56] as a part of a thermodynamic assessment of the Fe-Mn system, and we accepted this description of ${}^{E}G_m^{\gamma}$. The parameters ${}^{0}L^{\varepsilon}$ and ${}^{1}L^{\varepsilon}$ corresponding to the hcp phase were treated as constants and determined from our T_0 temperature data.

C. *Evaluation of T_0 Temperatures and Extrapolation to Pure Fe*

Lacking any evidence of the applicability of Eq. [5] in the presence of magnetic effects, we restricted its use to the range of Mn contents, where both A_s and M_s vary linearly with composition, *i.e.,* only to the alloys with 13.7 pct < wt pct Mn < 21.9 pct. The resulting T_0 values can be represented by the equation

$$T_0\ (\mathrm{K}) = (550 \pm 18) - (6.0 \pm 1) W_{\mathrm{Mn}} \qquad [11]$$

According to this expression, if the T_0 *vs* composition function for the fcc/hcp transformation remains linear in the low-Mn range of the system, one would have $T_0 = (550 \pm 18)$ K for pure Fe. This value coincides, by definition, with the temperature for the fcc/hcp equilibrium at 1 atm. This equilibrium in Fe is stable only at high pressures, but an extrapolation based on the Murnaghan equation of state[97] was performed by Fernández Guillermet and Gustafson,[54] who obtained $T_0 = 520$ K at 1 atm. This temperature is only (30 ± 18) K lower than the value given by the present extrapolation. In contrast, the thermodynamic description of Fe developed by Kaufman and co-workers[50,51,59,98] predicts a considerably lower value, *viz.,* $T_0 = 390$ K. Kaufman's value is the result of an elaborate treatment of various kinds of information. As a consequence, it is difficult to know whether their fcc/hcp metastable equilibrium temperature was controlled mainly by the high-pressure data[51] or by the data on the phase diagram and martensitic transformations in the Fe-Ru system.[51,99,100] Still, we note that the slope of the fcc/hcp equilibrium line in Kaufman's calculated *T vs P* phase diagram for Fe[99,98] is larger than the experimental,[101] and it seems evident that a better agreement with the high-pressure experiments could be achieved by increasing their fcc/hcp metastable equilibrium temperature at $P = 1$ atm. This would bring their T_0 closer to our result, without necessarily contradicting the T_0 data in Fe-Ru alloys.[99,51] Alternatively, we note that in order to reconcile the present data on T_0 for alloys with Kaufman's value for Fe, it is necessary that the T_0 line in the Fe-Mn system deviates rapidly from the linear behavior at low Mn contents. A direct experimental verification of this hypothesis is hampered by the fact that the bcc phase predominates in the products of the martensitic transformation of the fcc phase. However, even if one could postulate, *e.g.,* on theoretical grounds, a physical effect responsible for such nonlinearity of the T_0 line and thereby conclude that the present value $T_0 = (550 \pm 18)$ K is too high, it would remain to be explained why the extrapolation in the *T vs P* phase diagram of pure Fe[54] gives a close result. In view of these facts, the description of Fe given in Reference 54 was used to analyze the present results.

D. *Composition Dependence of T_0 at High Mn Contents*

Among the various thermodynamic quantities introduced in Section A, only two remain to be discussed. The first quantity is the parameter $\beta_{\mathrm{Fe,Mn}}^{\gamma}$, which is related to the magnetic entropy of the fcc phase (Eq. [8]), and the second is the excess Gibbs energy of the hcp phase, which is described by the parameters ${}^{0}L^{\varepsilon}$ and ${}^{1}L^{\varepsilon}$ (Eq. [10]). The first quantity can only be determined from information on the magnetic entropy of Fe-Mn alloys, which is obtained from measurements of the heat capacity. This type of information is available from the work by Hashimoto and Ishikawa[77] only for Mn contents that are larger than the compositions of interest in the present study. Therefore, we did not use their[77] data, but we explored the effect of changing $\beta_{\mathrm{Fe,Mn}}^{\gamma}$

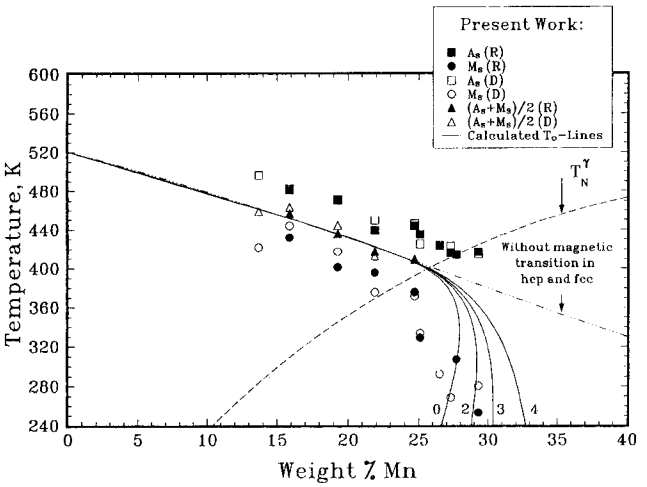

Fig. 19—The composition dependence of the T_0 temperature (solid line), defined by Eq. [4], calculated by adopting various values of the $\beta^{\gamma}_{Fe,Mn}$ parameter (Eq. [9]) that determines the total magnetic entropy (Eq. [8]), compared with experimental values of A_s (squares) and M_s (circles) obtained in the present work. The triangles refer to T_0 temperature values estimated as $T_0 = (A_s + M_s)/2$ (Eq. [5]). The dashed-dotted line represents the calculated T_0 temperature corresponding to the case in which neither fcc nor hcp present a magnetic transition. The dashed line labeled T_N^{γ} describes the composition dependence of the Néel temperature of the fcc phase according to the phenomenological representation reported by Huang.[56]

Table III. Total Magnetic Entropy of fcc Fe-Mn Alloys of 30, 40, and 50 At. Pct Mn, According to a Calculation Based on Eqs. [8] and [9], with the Known $^0\beta^{\gamma}_{Fe}$ and $^0\beta^{\gamma}_{Mn}$ (Section V) and $^0\beta^{\gamma}_{Fe,Mn} = 3$, Compared with the Values Extracted by Hashimoto and Ishikawa [77] from *Cp* Data

	Magnetic Entropy (Eq. [8]) (J/K·mol)	
Mn Content (At. Pct)	Present Estimate (Using $\beta^{\gamma}_{Fe,Mn} = 3$)	Hashimoto and Ishikawa [77] (From *Cp* Data)
30	3.2	5.8
40	3.0	3.7
50	2.9	2.5

in a series of calculations where this parameter was varied systematically so that we covered the range of magnetic entropies that are expected from Reference 77. In each of these calculations, $\beta^{\gamma}_{Fe,Mn}$ was given a value, and then the $^0L^{\varepsilon}$ and $^1L^{\varepsilon}$ parameters were evaluated using the T_0 temperatures estimated in the previous section. The analysis was performed by means of a computer optimization program,[102] which minimizes the square sum of the differences between experimental and calculated values for T_0.

A comparison between experiments and calculations is given in Figure 19, where we plot the T_0 lines obtained with $\beta^{\gamma}_{Fe,Mn}$ values increasing between 0 and 4, which corresponds to decreasing magnetic entropies. In addition, we plot the T_0 line corresponding to the hypothetical case where there is no magnetic transition in fcc or hcp, which was simulated by setting equal to zero the Néel temperatures of both phases. Figure 19 demonstrates that the T_0 line calculated by means of the present models accounts well for the composition dependence of the points obtained as $(A_s + M_s)/2$ from our measurements (triangles). These calculations also show that one can reproduce equally well the experiments in the linear part of the T_0 line by using different values for the parameter $\beta^{\gamma}_{Fe,Mn}$, which is natural, because in this range, the fcc phase remains in the paramagnetic state. In addition, our calculations predict that T_0 deviates rapidly from the linear behavior for Mn contents just to the right of the point where $T_0 = T_N^{\gamma}$.

Since the approximation $T_0 = (A_s + M_s)/2$ was not applied to alloys having at least one of the transformation temperatures in the antiferromagnetic range of fcc, we cannot use the present measurements to directly identify the true T_0 line among the various possibilities shown in Figure 19. However, by relying on the definition of T_0 and its qualitative relation to M_s and A_s, one could estimate a range of probable $\beta^{\gamma}_{Fe,Mn}$ values, *i.e.*, of probable magnetic entropies. For the transformation to occur on cooling, it is necessary that $T_0 > M_s$; *i.e.*, the true T_0 line for the Fe-Mn system should fall to the right of the data points representing an fcc → hcp transformation. According to the results in Figure 19, this condition starts to be fulfilled when $\beta^{\gamma}_{Fe,Mn}$ falls somewhere between 2 and 3. To see how this result compares with the available magnetic entropy data, we compare in Table III the entropies reported by Hashimoto and Ishikawa[77] for alloys containing 30, 40, and 50 at. pct Mn, with the values one would get by using Eqs. [8] and [9] and the tentative value $\beta^{\gamma}_{Fe,Mn} = 3$. It is encouraging that two of the three results from Reference 77 are reasonably well accounted for by the calculation.

E. *Final Comparisons with Previous Work*

A thermodynamic calculation of the fcc/hcp T_0 line was reported long ago by Breedis and Kaufman.[53] Their calculation predicted a possible range for the fcc ↔ hcp transformation extending up to Mn contents of about 50 at. pct Mn. In the work by Rabinkin,[49] an attempt was made to account for magnetic effects in the γ and ε phases. His analysis also predicted a range for the fcc ↔ hcp transformation larger than that reported in References 12, 21, and 82. Gartstein and Rabinkin[24] studied the $\gamma \rightarrow \varepsilon$ transformation in Fe-Mn alloys using transmission electron microscopy and found small needles of the ε phase in quenched alloys with 37.2 at. pct Mn, which falls outside the composition range where the transformation has been detected (Figure 15) and the range predicted by the calculations in Figure 19. Additional observations of the formation of small amounts of ε at large Mn contents were reported by Rabinkin *et al.*,[103] from a Mössbauer spectroscopy study of a quenched Fe-37.2 at. pct Mn alloy, and by Gulyaev *et al.*,[39] from an electron microscopy study of an Fe-29.5 wt pct Mn alloy. However, neither in these works[39,103] nor in that of Gartstein and Rabinkin[24] is there conclusive evidence that the martensite phase observed was induced only by cooling.

Finally, we shall compare the present results with those obtained by Huang[56] as a part of the assessment of the Fe-Mn system. Huang analyzed the fcc/hcp metastable equilibria, using the models described in this section, but described the β^{γ} parameter by neglecting the third term of the right-hand side in Eq. [9]. This approximation is not supported by the present work, where we find that the M_s temperatures for alloys with more than about 25 pct Mn cannot be reconciled with calculations of T_0 without accepting that $\beta^{\gamma}_{Fe,Mn}$ is of the order of 3. As a consequence, the T_0 line calculated by using Huang's description of the

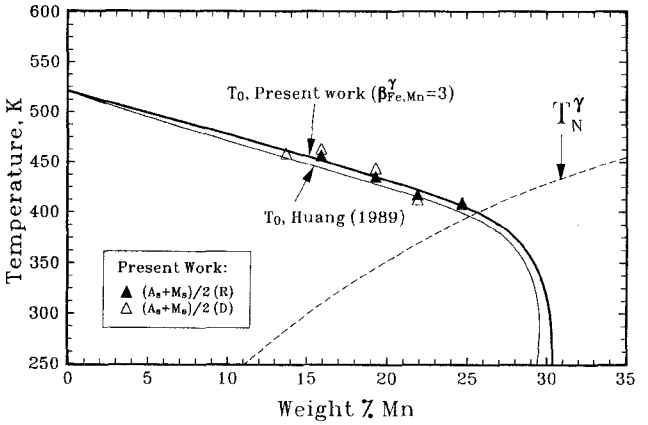

Fig. 20—The composition dependence of the T_0 temperature, defined by Eq. [4], calculated in the present work by adopting the value $\beta^{\gamma}_{Fe,Mn} = 3$ (thick solid line) and by relying on the thermodynamic description of γ an ε presented by Huang[56] (thin solid line). T_0 temperature values estimated from the present results for A_s and M_s as $T_0 = (A_s + M_s)/2$ (Eq. [5]) are shown. The dashed line labeled T^{γ}_{N} describes the composition dependence of the Néel temperature of the fcc phase according to the phenomenological representation reported by Huang.[56]

fcc phase falls to the left of the one we calculate by taking $\beta^{\gamma}_{Fe,Mn} = 3$. This is demonstrated in Figure 20.

ACKNOWLEDGMENTS

The authors would like to thank Drs. M. Ahlers, L. Kaufman, F. Lovey, J. Van Humbeeck, and Professor A. P. Miodownik for discussions and comments on the present study. One of us (MS) would like to thank Professor E. Hornbogen for introducing him to the field of shape memory effects in Fe-based alloys. Dr. W. Huang provided us with data files on the Fe-Mn system. Dr. B. Skrotzki provided us with a copy of her thesis. We also acknowledge the valuable assistance of many colleagues during the experimental part of the work. In particular, C. Ayala and H. Peretti helped us with the fabrication of the alloys, and C. Gómez and T. Carrasco helped with the preparation of the samples. F. Fürst and C. Klenner made the quartz capsules. Thanks are due to M. Arribére for the neutron activation study, to C. Pasquevich for the atomic absorption determinations, and to S. Dutrús for the microprobe measurements. A. Baruj and Lic. M. Prado kindly helped us with some of the measurements. The manuscript was typed by N. Mackern and A. Cohen at the Publications Section of the Centro Atómico Bariloche (CAB). Ing. P. Bavdaz designed the dilatometer used in this work. Its mechanical parts were made by F. Tutzauer. The dilatometer was constructed in the workshops of the CAB, with financial support from the A. von Humboldt Foundation. Grants from the Fundación Balseiro and the Consejo Nacional de Investigaciones Científicas y Técnicas of Argentina (CONICET), PID No. 3289/92, are gratefully acknowledged. The work by one of us (AFG) is part of a research project supported by the CONICET, under grant No. PIA-0028/92.

REFERENCES

1. W. Schmidt: *Arch. Eisenhüttenwes.*, 1929, vol. 4, pp. 293-300.
2. E. Öhman: *Z. Phys. Chem. B*,1930, vol. 8, pp. 81-110.
3. F.M. Walters, Jr. and C. Wells: *Trans. Am. Soc. Met.*, 1935, vol. 23, pp. 727-50.
4. A.R. Troiano and F.T. McGuire: *Trans. Am. Soc. Met.*, 1943, vol. 31, pp. 340-64.
5. J. Gordon Parr: *J. Iron Steel Inst.*, 1952, vol. 171, pp. 137-41.
6. M. Hansen and K. Anderko: *Constitution of Binary Alloys,* McGraw Hill, New York, NY, 1958, pp. 664-68.
7. C.H. White and R.W.K. Honeycomb: *J. Iron Steel Inst.*, 1962, vol. 200, pp. 457-66.
8. I.N. Bogachev, V.F. Yegolayev, and L.S. Malinov: *Phys. Met. Metall.*, 1963, vol. 16, pp. 44-49.
9. H. Schumann: *Neue Hütte,* 1965, vol. 10, pp. 429-33.
10. H. Schumann: *Neue Hütte,* 1966, vol. 11, pp. 299-303.
11. R.Sh. Shklyar, V.F. Yegolayev, L.D. Chumakova, L.S. Malinov, and V.D. Solovey: *Phys. Met. Metall.*, 1966, vol. 21, pp. 75-80.
12. H. Schumann: *Arch. Eisenhüttenwes.*, 1967, vol. 8, pp. 647-56.
13. H. Schumann: *Arch. Eisenhüttenwes.*, 1967, vol. 9, pp. 743-49.
14. H. Schumann: *Z. Metallkd.*, 19, vol. 58, pp. 207-10.
15. H. Schumann: *Arch. Eisenhüttenwes.*, 1969, vol. 40, pp. 1027-37.
16. A. Holden, J.D. Bolton, and E.R. Petty: *J. Iron Steel Inst.*, 1971, vol. 209, pp. 721-28.
17. L.N. Andryushchenko and L.Ya. Georgiyeva: *Phys. Met. Metall.*, 1972, vol. 33, pp. 156-65.
18. I.N. Bogachev and G.E. Zvigintseva: *Sov. Phys. Dokl.*, 1974, vol. 19, pp. 153-54.
19. H. Schumann: *Neue Hütte,* 1974, vol. 19, pp. 166-70.
20. I.N. Bogachev, M.S. Khadyev, and Yu.R. Nemirovskiy: *Phys. Met. Metall.*, 1975, vol. 40, pp. 69-77.
21. H. Schumann: *Praktische Metall.*, 1975, vol. 12, pp. 511-25.
22. A.P. Gulyaev, T.F. Volynova, and I.Ya. Georgieva: *Met. Sci. Heat Treat.*, 1978, vol. 20, pp. 179-82.
23. F. Trichter, A. Rabinkin, M. Ron, and A. Sharfstein: *Scripta Metall.*, 1978, vol. 12, pp. 431-34.
24. E. Gartstein and A. Rabinkin: *Acta Metall.*, 1979, vol. 27, pp. 1053-64.
25. K. Enami, A. Nagasawa, and S. Nenno: *Scripta Metall.*, 1975, vol. 9, pp. 941-48.
26. A. Sato, E. Chishima, K. Soma, and T. Mori: *Acta Metall.*, 1982, vol. 30, pp. 1177-83.
27. A. Sato, K. Soma, E. Chishima, and T. Mori: *J. Phys., Colloq. C4,* 1982, vol. 43, pp. 797-802.
28. A. Sato, E. Chishima, Y. Yamaji, and T. Mori: *Acta Metall.*, 1984, vol. 32, pp. 539-47.
29. A. Sato, Y. Yamaji, and T. Mori: *Acta Metall.*, 1986, vol. 34, pp. 287-94.
30. M. Murakami, H. Otsuka, H.G. Suzuki, and S. Matsuda: *Proc. Int. Conf. on Martensitic Transformations,* The Japan Institute of Metals, Tokyo, 1987, p. 985–90.
31. M. Sade, K. Halter, and E. Hornbogen: *Z. Metallkd.*, 1988, vol. 79, pp. 487-91.
32. P. Donner, E. Hornbogen, and M. Sade: *J. Mater. Sci. Lett.*, 1989, vol. 8, pp. 37-40.
33. G. Ghosh, Y. Vanderveken, J. Van Humbeeck, M. Chandrasekaran, L. Delaey, and W. Vanmoorleghem: *Proc. MRS Int. Meet. on Advanced Materials,* Materials Research Society, Pittsburgh, PA, 1989, vol. 9, pp. 457-62.
34. M. Murakami and H. Otsuka: *Proc. MRS Int. Meet. on Advanced Materials,* Materials Research Society, Pittsburgh, PA, 1989, vol. 9, pp. 447-50.
35. H. Otsuka, M. Murakami, and S. Matsuda: *Proc. MRS Int. Meet. on Advanced Materials,* Materials Research Society, Pittsburgh, PA, 1989, vol. 9, pp. 451-56.
36. A. Sato: *Proc. MRS Int. Meet. on Advanced Materials,* Materials Research Society, Pittsburgh, PA, 1989, vol. 9, pp. 431-45.
37. M. Sade, K. Halter, and E. Hornbogen: *J. Mater. Sci. Lett.*, 1990, vol. 9, pp. 112-15.
38. Y. Tomota, M. Piao, T. Hasunuma, and Y. Kimura: *J. Jpn. Inst. Met.*, 1990, vol. 54, pp. 628-34.
39. A.A. Gulyaev, E.Z. Vintaikin, E.L. Svistunova and A.B. Oralbaev: *Met. Sci. Heat Treat.*, 1991, vol. 33, pp. 574-77.
40. L. Jian and C.M. Wayman: *Scripta Metall. Mater.*, 1992, vol. 27, pp. 279-84.
41. C.F. Chen, J.H. Yang, and L.C. Zhao: *Proc. MRS Int. Meet. on Advanced Materials,* Materials Research Society, Pittsburgh, PA, 1989, vol. 9, pp. 481-86.
42. H. Otsuka, H. Yamada, T. Maruyama, H. Tanahashi, S. Matsuda,

and M. Murakami: *Iron Steel Inst. Jpn. Int.,* 1990, vol. 30, pp. 674-79.
43. A.A.H. Hamers and C.M. Wayman: *Scripta Metall. Mater.,* 1991, vol. 25, pp. 2723-28.
44. H. Inagaki: *Z. Metallkd.,* 1992, vol. 83, pp. 97-104.
45. J.H. Yang, H. Chen, and C.M. Wayman: *Metall. Trans. A,* 1992, vol. 23A, pp. 1431-37.
46. A. Fernández Guillermet: *Z. Metallkd.,* 1989, vol. 80, pp. 83-94.
47. L. Kaufman and M. Cohen: *Prog. Met. Phys.,* 1958, vol. 7, pp. 165-246.
48. L. Kaufman and M. Hillert: in *Martensite,* G.B. Olson and W.S. Owen, eds., ASM INTERNATIONAL, Materials Park, OH, 1992, pp. 41-58.
49. A. Rabinkin: *CALPHAD,* 1979, vol. 3, pp. 77-84.
50. L. Kaufman, E.V. Clougherty, and R.J. Weiss: *Acta Metall.,* 1963, vol. 11, pp. 323-35.
51. L.D. Blackburn, L. Kaufman, and M. Cohen: *Acta Metall., 1965,* vol. 13, pp. 533-41.
52. R.J. Weiss and K.J. Tauer: *J. Phys. Chem. Solids,* 1958, vol. 4, pp. 135-43.
53. J.F. Breedis and L. Kaufman: *Metall. Trans.,* 1971, vol. 2, pp. 2359-71.
54. A. Fernández Guillermet and P. Gustafson: *High Temp. High Pressures,* 1985, vol. 16, pp. 591-610.
55. A Fernández Guillermet and W. Huang: *Int. J. Thermophys.,* 1990, vol. 11, pp. 949-69.
56. W. Huang: *CALPHAD,* 1989, vol. 13, pp. 243-52.
57. G. Inden: *Phys. B,* 1981, vol. 103, pp. 82-100.
58. M. Hillert and M. Jarl: *CALPHAD,* 1978, vol. 2, pp. 227-38.
59. L. Kaufman: *Scand. J. Metall.,* 1991, vol. 20, pp. 32-38.
60. Z. Nishiyama: in *Martensitic Transformations,* M.E. Fine, M. Meshii, and C.M. Wayman, eds., Academic Press, New York, NY, 1978.
61. S. Cotes, M. Sade, and A. Fernández Guillermet: Centro Atómico Bariloche, 8400 S.C. de Bariloche, Argentina, unpublished research, 1993.
62. Y. Tomota, M. Strum, and J.W. Morris: *Metall. Trans. A,* 1986, vol. 17A, pp. 537-47.
63. I.N. Bogachev, G.Ye. Zvigintseva, V.F. Yegolayev, and G.I. Lyapunov: *Phys. Met. Metall.,* 1969, vol. 28, pp. 59-65.
64. A. Baruj, S. Cotes, M. Sade, and A. Fernández Guillermet: Centro Atómico Bariloche, 8400 S.C. de Bariloche, Argentina, unpublished research, 1993.
65. F.M. Walters, Jr. and M. Gensamer: *Trans. Am. Soc. Met.,* 1932, vol. 19, pp. 608-23.
66. I.N. Bogachev and L.S. Malinov: *Phys. Met. Metall.,* 1962, vol. 14, pp. 27-31.
67. H. Umebayashi and Y. Ishikawa: *J. Phys. Soc. Jpn,* 1966, vol. 21, pp. 1281-94.
68. I.N. Bogachev, V.F. Yegolayev, G.Ye. Zvigintseva, and L.V. Zhuravel: *Phys. Met. Metall.,* 1969, vol. 28, pp. 125-30.
69. M. Fujita and I. Uchiyama: *Tetsu-to-Hagané,* 1974, vol. 60, pp. 525-39.
70. K. Ishida and T. Nishizawa: *Trans. Jpn. Inst. Met.,* 1974, vol. 15, pp. 225-31.
71. I.Ya. Georgiyeva, N.A. Sorokina, and V.I. Gal'tsova: *Phys. Met. Metall.,* 1981, vol. 49, pp. 178-81.
72. M. Tolba-Sallam, D. Georgeault, and C. Cizeron: *Scripta Metall.,* 1981, vol. 15, pp. 849-52.
73. J.T. Lenkkeri and J. Levoska: *Phil. Mag.,* 1983, vol. 48, pp. 749-58.
74. B. Skrotzki: Ph.D. Thesis, Fortschitt-Berichte VDI 5, 269, Düsseldorf VDI-Verlag, 1992.
75. S. Takaki, H. Nakatsu, and Y. Tokunaga: *Mater. Trans. JIM,* 1993, vol. 34, pp. 489-95.
76. H. Fujimori: *J. Phys. Soc. Jpn.,* 1966, vol. 21, pp. 1860-65.
77. T. Hashimoto and Y. Ishikawa: *J. Phys. Soc. Jpn.,* 1967, vol. 23, pp. 213-23.
78. Y. Ishikawa and Y. Endoh: *J. Phys. Soc. Jpn.,* 1967, vol. 23, pp. 205-13.
79. Y. Endoh and Y. Ishikawa: *J. Phys. Soc. Jpn.,* 1971, vol. 30, pp. 1614-27.
80. T.L. Frolova, L.P. Zhitova, and I.N. Bogachev: *Phys. Met. Metall.,* 1972, vol. 34, pp. 199-202.
81. G.G. Amigud, I.N. Bogachev, G.A. Dorofeyev, S.D. Karakishev, and V.S. Litvinov: *Phys. Met. Metall.,* 1973, vol. 36, pp. 208-10.
82. I.N. Bogachev, V.D. Kibal'nik, T.L. Frolova, and L.D. Chumakova: *Phys. Met. Metall.,* 1974, vol. 37, pp. 62-67.
83. Y. Ishikawa, H. Sekine, and K. Yamada: *J. Phys. Soc. Jpn.,* 1974, vol. 37, p. 874.
84. H.H. Ettwig and W. Pepperhoff: *Phys. Status Solidi A,* 1974, vol. 23, pp. 105-11.
85. L. Remy and A. Pineau: *Mater. Sci. Eng.,* 1977, vol. 28, pp. 99-107.
86. Y. Endo, Y. Noda, and M. Iizumi: *J. Phys. Soc. Jpn.,* 1981, vol. 50, pp. 469-75.
87. W. Stamm, H. Zähres, M. Acet, K. Schletz, and E.F. Wasserman, private communication. Tieftemperaturephysik, Universität Duisburg, D 4100 Duisburg, FRG.
88. R.J. Salzbrenner and M. Cohen: *Acta Metall.,* 1979, vol. 27, pp. 739-48.
89. H. Warlimont, L. Delaey, R.V. Krishnan, and H. Tas: *J. Mater. Sci.,* 1974, vol. 9, pp. 1545-55.
90. A. Fernández Guillermet: *High Temp. High Pressures,* 1987, vol. 19, pp. 477-99.
91. A. Fernández Guillermet: *Z. Metallkd.,* 1987, vol. 78, pp. 639-47.
92. M. Hillert: in *Computer Modeling of Phase Diagrams,* L.H. Bennett, ed., TMS-AIME, Warrendale, PA, 1986, pp. 1-17.
93. H. Ohno and M. Mekata: *J. Phys. Soc. Jpn.,* 1971, vol. 31, pp. 102-108.
94. K.J. Tauer and R.J. Weiss: *Phys. Rev.,* 1955, vol. 100, pp. 1223-24.
95. J.A. Hofmann, A. Paskin, K.J. Tauer, and R.J. Weiss: *J. Phys. Chem. Solids,* 1956, vol. 1, pp. 45-60.
96. O. Redlich and A.T. Kister: *Ind. Eng. Chem.,* 1948, vol. 40, pp. 345-48.
97. A. Fernández Guillermet, P. Gustafson, and M. Hillert: *J. Phys. Chem. Solids,* 1985, vol. 46, pp. 1427-29.
98. L. Kaufman and H. Bernstein: *Computer Calculation of Phase Diagrams,* Academic Press, New York, NY, 1970.
99. L. Kaufman: Special Report No. 93, Iron and Steel Institute, London, 1965, pp. 48-52.
100. G.L. Stepakoff and L. Kaufman: *Acta Metall.,* 1968, vol. 16, pp. 13-22.
101. F.P. Bundy: *J. Appl. Phys.,* 1965, vol. 36, pp. 616-20.
102. B. Jansson: Ph.D. Thesis, The Royal Institute of Technology, Stockholm, 1984.
103. A Rabinkin, M. Ron, F. Trichter, and E. Gartstein: *Proc. Int. Conf. on Martensitic Transformations, ICOMAT 79,* Cambridge, MA, 1979, pp. 300-05.